Asia-Pacific Journal of Science and Technology: Volume: 27. Issue: 03. Article ID.: APST-27-03-02. Research Article

APST

Asia-Pacific Journal of Science and Technology

https://www.tci-thaijo.org/index.php/APST/index

Published by the Research and Technology Transfer Affairs Division,
Khon Kaen University, Thailand

The feasibility of Sentinel-2A and Landsat 8 imagery in rock outcrop extraction using object-based oriented classification

Doan Ngoc Nguyen Phong[1], Do Thi Viet Huong[1,*], Nguyen Quang Tuan[1], Do Quang Thien[2], Nguyen Phuoc Gia Huy[3] and Bui Thi Thu[1]

[1]Department of Natural Resources - Environmental Management and GeoInformatic, Faculty of Geography and Geology, University of Sciences, Hue University, Hue City, Vietnam
[2]Department of Engineering Geology and Hydro-Geology, Faculty of Geography and Geology, University of Sciences, Hue University, Hue City, Vietnam
[3]Thua Thien Hue Center of Information Technology, Hue City, Vietnam
[*]Corresponding author: dtvhuong@hueuni.edu.vn

Received 17 September 2021
Revised 27 December 2021
Accepted 8 January 2022

Abstract

The presence of exposed rocks in the mountainous areas of the Thua Thien Hue province in Vietnam has affected the expansion of agroforestry farming areas. A novel classification approach is proposed to extract rock outcrops in the mountainous region by integrating the object-based oriented classification (OBOC) method and multiple ratio image indices. The default index (mean Near-infrared - NIR, mean Blue, Brightness) and calculated index (normalized difference built-up index - NDBI, normalized difference vegetation index - NDVI, topsoil grain size index - TGSI) ratio images effectively integrate delineating rock outcrops through the determination of the threshold of image index values. The main findings are that Sentinel-2A and Landsat 8 provided an acceptable extraction of exposed rocks in the mountainous area with an overall accuracy of over 80% based on the OBOC technique. Sentinel-2A extracted the revealed rocks with higher accuracy than Landsat 8 in two test sites of the mountainous region of the Thua Thien Hue province. The results were verified in the field, demonstrating that rock outcrops were better detected by Sentinel-2A (93%) than Landsat 8 (86%), in agreement with existing map soil data published in the geographic information system of the Thua Thien Hue province (GISHue data). Furthermore, Sentinel-2A data revealed specific sites with outcropping rocks which were not included, yet yielded reliable field results confirming its potential for mapping and monitoring exposed rocks for environmental protection and agroforestry development in mountainous areas.

Keywords: Exposed rock, TGSI, NDVI, NDBI, Mountainous areas

1. Introduction

Remote sensing has become increasingly significant in soil mapping and monitoring land use/land cover (LULC). The extraction and mapping of rock outcrop areas are crucial for geological, engineering, and industrial applications, as well as environmental protection and agroforestry development [1-3]. Although occupying only small proportion of LULC, exposed rocks are considered crucial objects that influence soil formation, geomorphology, and natural and environmental hazards. Exposed rocks are widespread in areas where soil erosion is quicker than weathering or where exposed rocks are generated by artificial facilities and subsequent soil and rock removal from some areas [1].

The mountainous area of Vietnam, which mainly has a rocky mountain terrain type, has always been the main focus on land use in a suitable way for sustainable socio-economic development. However, due to the diversity of landscapes in mountainous regions, spatial planning for its socio-economic development is challenging to organise.

The exposed rocks are distributed randomly and discontinuously among LULC and sparsely among outcropping terrains, which are hard to define through field investigations. The emergence of remote sensing image applications allows the automatic extraction/classification of LULC, rock outcrops, and other rock-mineral components [4-6]. Besides, many sources with different spatial resolutions such as remotely piloted aircraft system images, unmanned aerial vehicles, Radarsat-1, Advanced Land Observing Satellite (ALOS) imagery, Landsat 8, Sentinel-2A, ASTER GDEM, Earth Observing 1 (EO-1) Hyperion, and simulated Earth Observing System (EOS) Terra ASTER imageries have been used to distinguish exposed rocks from other land covers [1, 7-11].

Various approaches have been applied to extract rocky outcrops. These have included: integrating a dimidiate pixel model and spectral mixture analyses through accuracy improvement with ALOS images in karst regions 0; building a specific exposed rock index using the near-infrared band and shortwave infrared-2 bands of Landsat 8 reflectance data [6]; combining the use of spectral patterns, normalised difference vegetation index (NDVI), normalized difference vegetation index - spectral mixture analysis (NDVI-SMA), modified normalised difference water index (MNDWI), normalised difference snow index (NDSI) images, topographical analysis, multifractal algorithms with Sentinel-2A MSI, advanced spaceborne thermal emission and reflection radiometer global digital elevation model (ASTER GDEM), Hyperion, and simulated EOS Terra ASTER imageries [1, 12-14].

In the Thua Thien Hue province, the published exposed rock maps' database has been primarily derived and interpreted via traditional methods, including conducting soil surveys, sampling soil profiles, and observing the rock outcrops based on their position relative to the geology, landforms, topography, and natural vegetation. It has thus still not been updated and lacks a quality assessment [3]. The possibility of identifying exposed rocks from Landsat 8 was initially evaluated by integrating the automatic interpretation and threshold identification of image index values to extract exposed rocks from the other LULC types [3, 15]. However, when using a default ratio image such as Brightness, the Blue value can effectively separate the coastal sand strip from the bare land and the exposed rock areas in the case study area. Meanwhile, exposed rocks frequently occur in scattered hilly regions mixed with vegetation and barren land. Therefore, enhancing the ability to dissect exposed rocks directly requires a consideration of the appropriate calculation indices of the other satellite image data.

The objective of this study is first to explore the feasibility of Sentinel-2A and Landsat 8 imagery for extracting rock outcrops using the object-based oriented classification (OBOC) method. Second, the classification accuracies of two test sites of distinct mountainous areas of the Thua Thien Hue province, Vietnam, using Sentinel-2A and Landsat 8 were examined to assess the execution of the OBOC method with ratio index images including NDVI, normalised difference built-up index (NDBI), and topsoil grain size index (TGSI). The findings will update the existing dataset of exposed rocks, which can support the socio-economic development of the Thua Thien Hue province toward the digital transformation phase in natural resources and the environment up to 2025 and oriented to 2030.

2. Materials and methods

2.1 Study area and data

The presence of exposed rocks in the Thua Thien Hue province affects the organisation of urban planning to create material areas for socio-economic growth. Test site 1 (A Luoi) and test site 2 (Nam Dong) were chosen to examine the possibility of discriminating between exposed rocks and other LULC types located in the remote mountainous areas of Thua Thien Hue (Figure 1). Those regions are outlying districts, where long-term industrial crops are of great concern. Because this area has several fault lines, sections with rock outcrops are more evident than high terrains deeply buried in the sea [16]; hence, the evaluation was conducted in mountainous locations in the Thua Thien Hue province. The test sites are rectangular with a 3.5 km x 9.5 km area and are covered by significant LULC types (i.e., water bodies, built-up land, vegetation, bare land, and rock outcrops).

The Landsat 8 and Sentinel-2A scenes with free cloud covering the entire test sites of the mountainous area were collected to extract rock outcrops. Landsat 8 at Level -2 collected data on April 25, 2019 (path 125 Row 49), freely available from Earth Explorer (https://earthexplorer.usgs.gov/), providing 30 m spatial resolution optical imagery on eight spectral bands via the Operational Land Imager sensor and two bands via the Thermal Infrared Sensor.

The Sentinel image at Level-2A with a resolution of 20 x 20 m was collected on April 1, 2019 (T48TYD), which was downloaded freely from Land Viewer - EOS (https://eos.com/landviewer/). It includes spectral bands 2 - 7, 8A, 11, and 12, a true colour image (TCI), a scene classification map (SCL), an aerosol optical thickness (AOT), and water vapour (WV) map. In addition, base maps and existing soil datasets from the province were also supplemented for the analyses (Table 1).

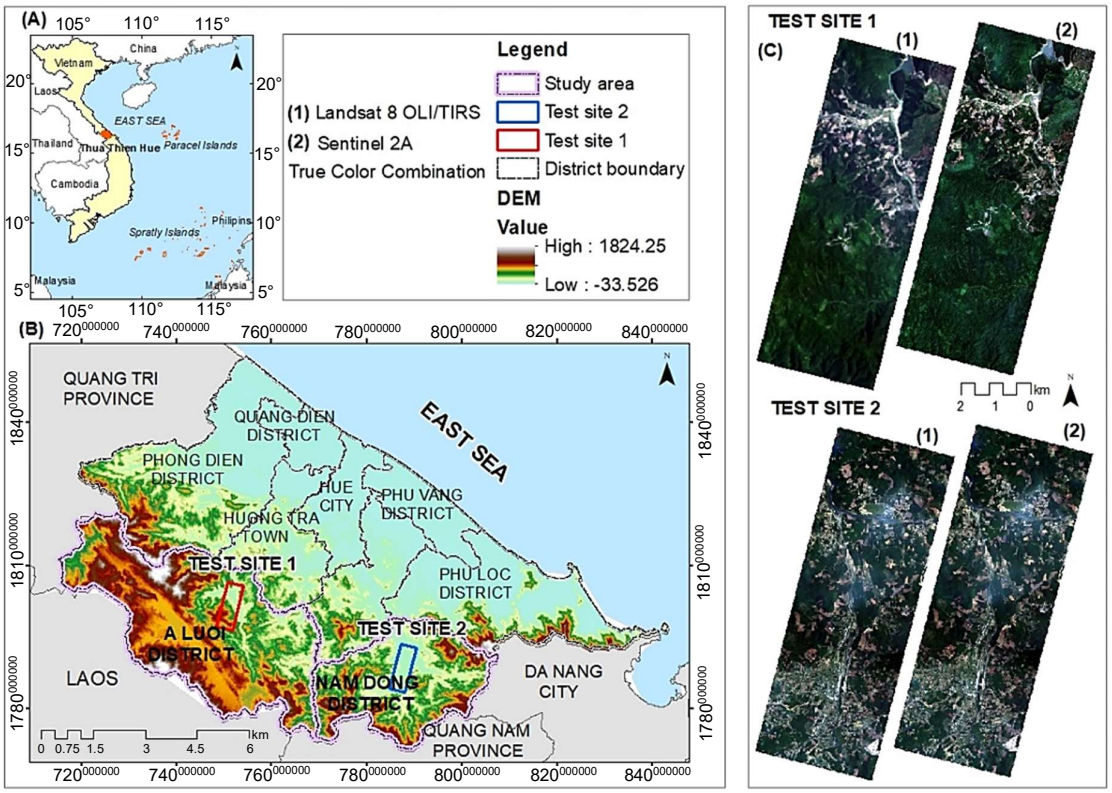

Figure 1 (A) Location of Thua Thien Hue Province in Vietnam; (B) Location of two test sites in the mountainous of Thua Thien Hue Province: Test site 1 (A Luoi district), Test site 2 (Nam Dong district); (C) The natural true color composition RGB - 432 for Sentinel-2A and Landsat 8 OLI/TIRS of the two test sites.

Table 1 Satellite images and GIS data utilized for extracting rock outcrops.

Data	Time	Resolution/Scale	Source
Landsat-8 OLI/TIRS (cloud 1, 48%)	25/04/2019	30 m	United States Geological Survey – (USGS) (https://earthexplorer.usgs.gov/)
Sentinel-2A	01/04/2019	20 m	European Space Agency- (ESA) (https://eos.com/landviewer/)
Base map	2019	1/10.000	GISHue database (Geodatabase)
Soil map	2003	1/100.000	

2.2 Methodology

By combining automatic classification and threshold values, the determination of index images allows the distribution of mixed and uncovered rocks in the sample region to be assessed in both satellite images. Because of its benefits over the conventional classification system, the deductive method used here is the OBOC process. This approach considers the graded object's spectral reflectance characteristics and other details, and has been shown to provide better classification results than the pixel-based method [17-19]. The process of rock outcrop extraction using an OBOC based on the flow chart is outlined in Figure 2.

In this study, both Landsat 8 OLI/TIRS and Sentinel-2 images were acquired in Level-2 processing and represent the corrected reflectance products. Therefore, the pre-processing phase is inherent including layer stacking, subset, and georeferencing. In Landsat 8, six bands were used for the layer stack; they are blue (450-510 nm), green (530-590 nm), red (640-670 nm), near infrared (NIR; 850-880 nm), shortwave infrared-1 (1570-1650 nm), shortwave infrared-2 (2110-2290 nm), and cirrus (1360-1380 nm). For Sentinel-2A, nine bands including Blue (490 nm), green (560 nm), red (665 nm), NIR (842 nm), four vegetation red edge bands (bands 5, 6, 7, and 8A), short wave infrared-1 (1610 nm), and short wave infrared-2 (2190 nm) were combined into a single image. The resample from a 20 m resolution to 30 m one was implemented for the Sentinel-2A image for comparison with Landsat 8. In addition, both Landsat 8 and Sentinel-2A were georeferenced using geographic coordinate system transformation and all images were projected from geographic coordinate system WGS 1984 to the

national VN-2000 coordinate system reference system projection. Subsequently, using the shapefile of a rectangle with a 3.5 km x 9.5 km area, spatial subsets of Landsat 8 and Sentinel-2A were obtained for the further processes (Figure 1C). The pre-process was conducted in ArcGIS Desktop version 10.4.

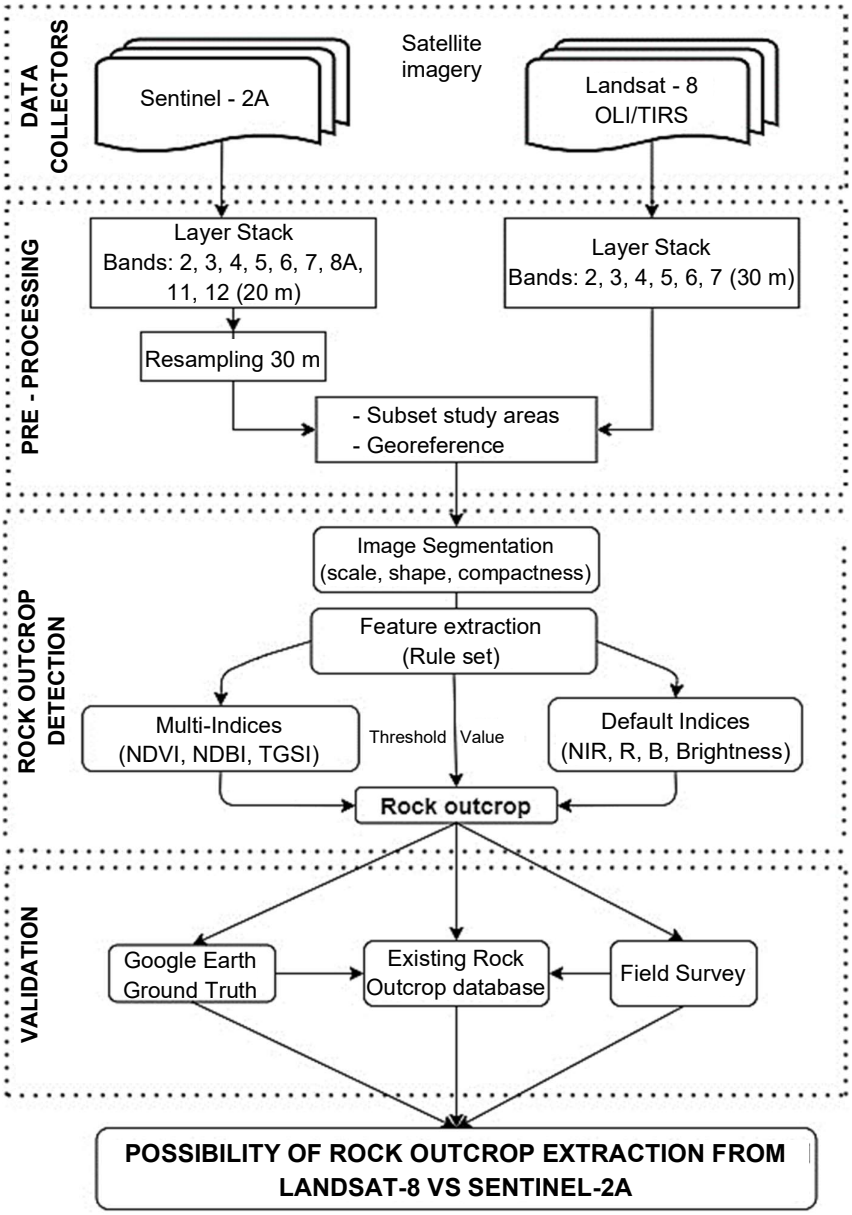

Figure 2 Workflow of the possibility of rock outcrop extraction Landsat-8 vs. Sentinel-2A.

The OBOC was implemented in the eCognition Developer 9.01 software in two steps: image segmentation and feature classification. First, the satellite image was segmented into small regions by aggregating the image pixels into spectrally homogenous image objects. The segmentation of images is based on defining the scale, shape, and compactness parameter of the object at each level of extraction through the Multiresolution Segmentation algorithm. The heterogeneity threshold is reached based on how weighted those parameters are to obtain the acceptable segmentation with distinct differences among the objects [5]. The classification method with assigned classes based on the membership function was adopted to classify the segments into different classes. The classified features were extracted following the defined rule set classification, mainly the threshold values of default indices (Brightness, mean NIR, mean Blue), and the calculated indices (NDBI, NDVI, and TGSI) were used to determine the exposed rock classes (Table 2).

Table 2 The indices used in the research.

Indices	Description	Formula	References Author
NDVI	Extract the vegetation coverage.	NDVI = NIR-RED/NIR+RED NDVI in the range [-1, +1]	[20, 21]
NDBI	Distinguish bare land from built-up land.	NDBI = SWIR-NIR/SWIR+NIR NDBI in range [-1, +1]	[14, 22]
TGSI	Determine soil texture and grain size, distinguish the rock outcrop from the bare land	TGSI = (RED - BLUE) /(RED+BLUE+GREEN) TGS in range [-1, +1]	[10]

A rule set of base classification followed the process of OBOC analysis to extract the rock outcrop areas at the final stage. On the Earth's surface, soil layers may be bare (loose rock, mixed rock, bare dirt, no topsoil) or coated with vegetation to various degrees. The reflected spectral radiant energy in bare soil comes from the soil surface and is usually attributed to soil properties and the form of the soil in which it occurs. The calculated reflectance distribution for partly vegetated soils is a mixture of soil and vegetation. Under the same environmental conditions, the more the soil layer is covered in the image, the more significant the contribution of the reflectance spectrum from the soil is, resulting in a decrease in the NDVI value with an increase in soil brightness [18]. The assigned class algorithm was applied through the trial and error process to find the realistic classification following the semantic rule set tree. The relevant cutting thresholds for the selected indices in each level were determined according to empirical values, the study area's internal characteristics, and the expert-based human knowledge of study area objects [5, 23].

The research used two indicators - overall accuracy and kappa statistics - to assess image classification accuracy. The kappa coefficient value is usually between 0 and 1, where $k \geq 0.8$ is highly accurate, $0.4 < k < 0.8$ defines a medium precision, and $k \leq 0.4$ represents a low precision [18, 24]. The image classification accuracy was evaluated using a grid of ground truth sample points from Google Earth at the time of image acquisition (April 30, 2019). In addition, a field survey was deployed for all the current rock outcrop datasets from the HueGIS database to check the actual conditions in the field test sites compared to the rock outcrop classification results from Landsat 8 and Sentinel-2A images. Based on the actual distribution of outcropping rocks from the GISHue database, the survey route at the two study sites was designed along the inter-provincial and district roads and trails through the plantations. The survey time was arranged in the dry season of April 2020, coinciding with the month of Landsat 8 and Sentinel-2A image collection. This phase was essential for supplementing and correcting exposed rock information for the soil database in the study area.

3. Results

3.1 Threshold and rules for extracting rock outcrops from ratio images

Both Landsat 8 and Sentinel-2A images were segmented on four scale levels (Table 3 and Figure 3). Multi-resolution segmentation utilised three parameters which were scale, shape, and compactness for the target LULC classes, i.e., waterbody, vegetated land, built-up land, bare land, and rock outcrop. The scale parameter defined the maximum degree of homogeneity of the feature segment; the higher values allowed more heterogeneity and and larger objects to be determined. While the shape size parameter defined the textural homogeneity (colour) of the resulting image objects, the remaining parameter of compactness defined whether the boundary of the segments should be smoother or more compact.

The value of each parameter varied through the levels of segmentation as: scale (1; 2; 3; 5), shape (0,2; 0,3; 0,4), and compactness (0,5; 0,7; 0,8). By keeping one or two parameters as constant, the trial and error process of the remaining parameter were experienced for obtaining the optimal parameter value.

For distinguishing the rock outcrops from the other objects, the scale parameters were experimented on by employing a trial and error strategy/process, and finally, their smallest value was defined as 1 in both Landsat 8 and Sentinel-2A due to the reality of their occurrence in scattered hilly regions and their shape size ranging from 100 m^2 to 1 ha or even 2-3 ha.

Considering the mountainous context of the two study sites, the compactness value varied from medium to higher values to achieve a high rate of smoothness of the defined objects. On the other hand, the shape values ranged from 0,1 to 0,4 with an equal step of 0,1 in both satellite images. The findings of the segmentation parameter in each level for the Sentinel-2A and the Landsat 8 are listed in Table 3.

The segmentation and rule set classification for the Sentinel-2A and Landsat 8 are presented in Table 3. The thresholds of default indices (mean NIR, mean Blue, Brightness) and calculated indices such as NDBI, NDVI, and TGSI were mainly used to define target classes in each Level of Landsat 8 and Sentinel-2A in the two test sites of the study area (Figure 3).

Table 3 Segmentation and rule set classification for extracting rock outcrop.

Level	Target class	Parameter threshold		Segmentation parameter (scale, shape, compactness)	
		Sentinel-2A	Landsat-8	Sentinel-2A	Landsat-8
Level 1	Water	Mean NIR≤1900	Mean NIR ≤ 12750	5; 0.3; 0.7	5; 0.3; 0.7
	Land	-	Mean Blue > 0		
Level 2	No Vegetable	NDVI < 0.37	NDBI ≤ - 0.07	3; 0.2; 0.5	3; 0.2; 0.5
	Veg	NDVI ≥ 0.37	NDBI > - 0.07		
Level 3	Built-up	NDBI ≥ 0.03	Brightness < 12030 & Mean Blue ≥ 10610	1; 0.4; 0.8	2; 0.2; 0.5
	Not Built-up	NDBI < 0.03	Brightness < 12030 & Mean Blue < 10610		
Level 4	Bare land	TGSI ≥ 0.0159	TGSI ≥ 0.02	1; 0.3; 0.7	1; 0.2; 0.5
	Rock outcrop	TGSI < 0.0159	TGSI < 0.02		

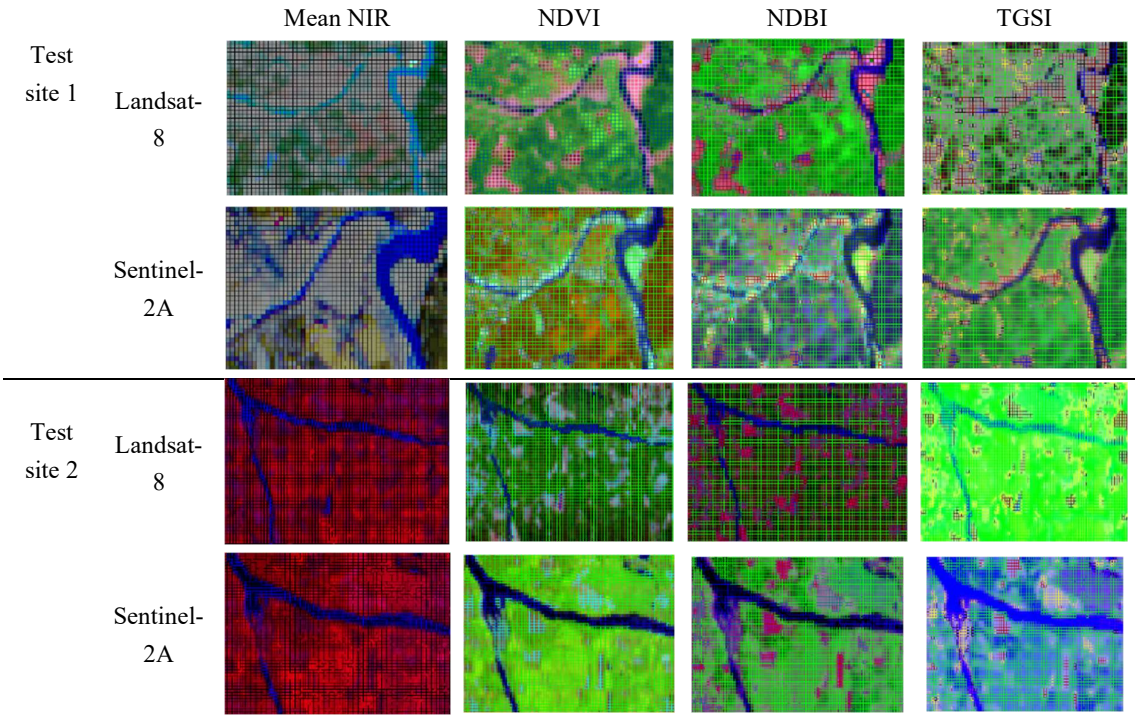

Figure 3 The segmentation levels and thresholds defined in Landsat-8 and Sentinel-2 images.

The object features were calculated in a multiresolution segmentation algorithm by evaluating the image objects via the layer value features using information derived from the spectral properties of the image objects. The layer value of the mean NIR band for both satellite images from Level 1 was used to extract water and land objects. However, for the Landsat 8 images, a lower layer value mean Blue band threshold was applied to remove land objects that were residual from the layer value mean NIR threshold. Then, NDVI and NDBI were used to discriminate between vegetated and non-vegetated objects such as construction lands, bare lands, and exposed rocks. Finally, the TGSI was applied to extract the exposed rock objects lying on barren ground, distinguishing things that were surface soil particles lifted from the land surface. The research region is a mountainous location with a lot of geological activity, and the TGSI is thus quite valuable for determining rock structures on the cover's surface.

The extraction of this information based only on NDVI, NDBI, mean Red, mean Blue, and Brightness resulted in mixed classification results between sand land and bare land. Therefore, the separation of those objects was more precise when using the Brightness index when sandy soil and bare soil properties were different. However, to filter out exposed rock objects within barren land, the TGSI was adequate to determine the soil particle sizes to remove the rocks mixed with the bare soil. The workflow chart of the object-based classification procedure is shown in Figure 4.

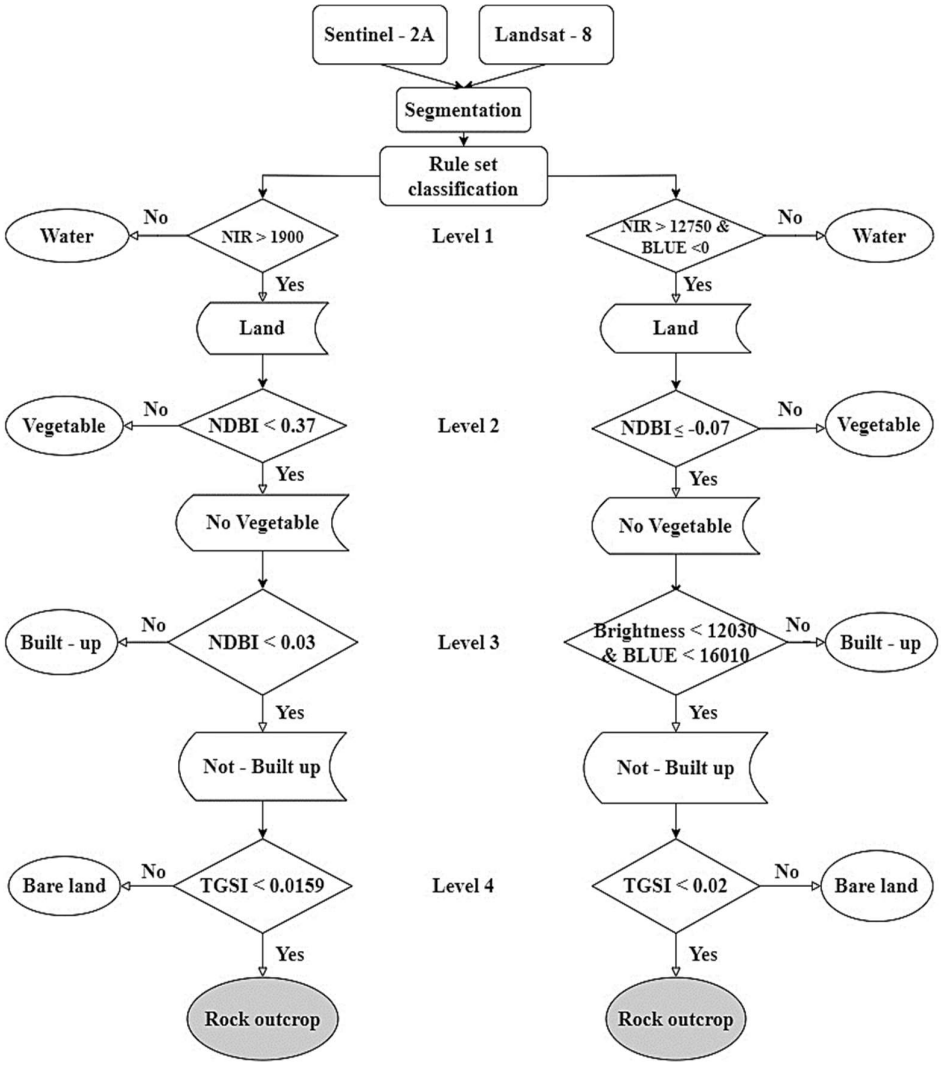

Figure 4 Workflow of the rule set object-based classification procedure defined in Landsat 8 and Sentinel-2A.

3.2 Rock outcrop extraction from Sentinel-2A and Landsat 8

Based on the OBOC method with the multiresolution segmentation algorithm approach, the rock outcrop classification over two test sites in Landsat 8 and Sentinel-2A images is shown in Figure 4, including five classes: water, built-up land, vegetation, bare land, and rock outcrops. The findings indicate that water and vegetation are the two objects that can be interpreted well in both Landsat 8 and Sentinel-2A images. A distinct difference and uncertainty arose from the two images of bare land, built-up land, and rock outcrops (Figure 5).

The rock outcrop area extracted from the Sentinel-2A image covers 9.11 km^2, which is more significant than in the Landsat 8 image (5.43 km^2) at test site two and has an area of 7.28 km^2 at test site 1, compared to the 4.32 km^2 area obtained from the Landsat 8 image.

Consequently, the difference in the area of the classes did not fluctuate much (less than 10 km^2). The accuracy assessment results were also more than 80% for both Landsat 8 and Sentinel-2A data. The findings indicate that water and vegetation are the two classes that can be interpreted well in both Landsat 8 and Sentinel-2A images. A distinct difference and uncertainty arose from the two images of bare land, built-up land, and rock outcrops.

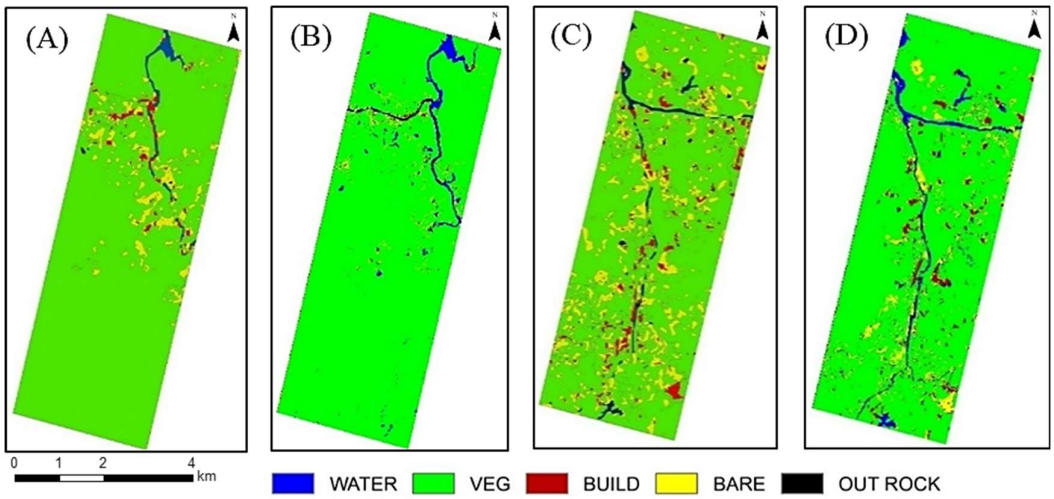

Figure 5 Rock outcrop extraction from Landsat 8 for the test site 1 (A) and test site 2 (C); from Sentinel-2 for test site 1 (B) and test site 2 (D).

In this research, to ensure the spatial homogeneity for the comparative extraction of rock information from Sentinel-2A and Landsat 8 data, the image preprocessing stage resampled the images into a resolution of 30 m x 30 m. The classification results were retrieved from the exact spatial resolution of the satellite images, but the difference in spectral reflectance characteristics affected the ability to distinguish the objects. When compared with Google Ground Truth data, the Sentinel-2A data gave more accurate results than Landsat 8. In the Landsat image, the built-up and bare land areas were more confused than in the Sentinel-2A one, leading to an entirely different extraction of exposed rock information. This misclassification arose because the image bands of Landsat 8, such as Brightness and NDBI, had close values, making it impossible to calculate a suitable threshold for each object (Figure 6, 7). The illustration of profiles 1 and 2 corresponds to the two results of Sentinel-2A and Landsat 8 classification, respectively (Figure 6A), which was shown clearly in the image of the landscape of rock outcrop staken from the field (Figure 6B) and the false-colour composition of Sentinel-2A (Figure 6C) and Landsat 8 (Figure 6D) for the areas 1 and 2, respectively.

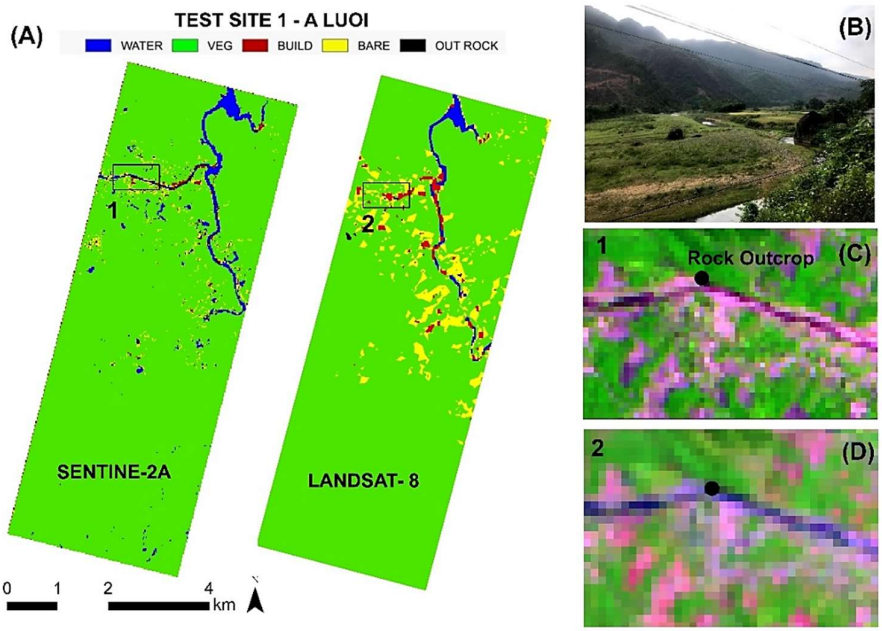

Figure 6 Illustration of rock outcrop extraction from Landsat 8 and Sentinel-2 for the test site 1- A Luoi: (A) result of rock outcrop classification from Sentinel-2A and Landsat 8; (B): landscape of rock outcrops in the field; false colour composition of Sentinel-2A (C) and Landsat 8 (D) for the areas 1 and 2, respectively.

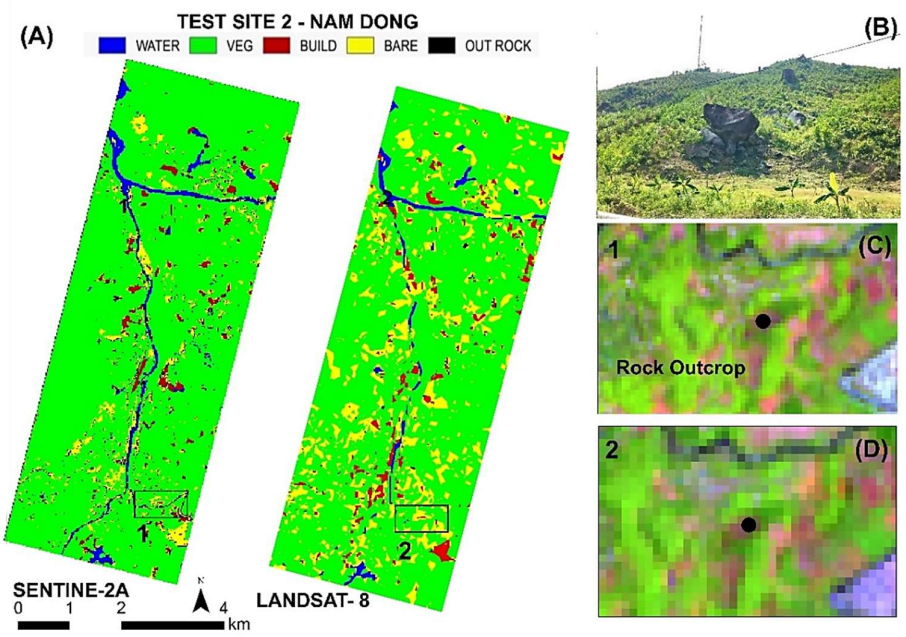

Figure 7 Illustration of rock outcrop extraction from Landsat 8 and Sentinel-2 for the test site 2- Nam Dong: (A) result of rock outcrop classification from Sentinel-2A and Landsat 8; (B): landscape of rock outcrops in the field; false colour composition of Sentinel-2A (C) and Landsat 8 (D) for the areas 1 and 2, respectively.

4. Discussion

The accuracy assessment results of rock outcrop classification for the two test sites in Sentinel-2A and Landsat 8 data are presented in Table 4.

Table 4 The result of classification accuracy assessment.

Class type	Kappa coefficient			
	Sentinel-2A		Landsat 8 OLI/TIRS	
	Test site 1	Test site 2	Test site 1	Test site 2
Built-up	0.89	0.89	0.82	0.83
Bare land	0.80	0.82	0.75	0.74
Water	0.91	0.89	0.86	0.81
Vegetation	0.87	0.85	0.82	0.88
Rock outcrop	0.79	0.72	0.69	0.72
Overall kappa coefficient	0.86	0.82	0.75	0.76
Overall classification accuracy	86.00%	84.00%	80.00%	81.00%

The overall accuracies of the OBOC method for Landsat 8 were 80% and 81% at test sites 1 and 2, respectively. The overall kappa coefficient values were 0.75 and 0.76 for test sites 1 and 2, respectively.

For Sentinel-2A data, the overall accuracy was 86% at test site 1 and 84% at test site 2, with a kappa value above 0.8 for both test sites. Sentinel-2A had a better overall kappa coefficient for the rock outcrop objects than Landsat 8 (with a value above 0.7 at both test sites). The Landsat 8 kappa value was significantly lower, implying a reduced confidence level in the extraction of all the classes, mainly the exposed rocks (0.69). There was also a notable gap in the overall classification accuracy, with the Landsat 8 data having more inaccurate scores than the Sentinel-2A image data.

The feasibilities of Sentinel-2A and Landsat 8 data for exposed rock extraction using OBOC were further evaluated by comparing accurate survey results. The survey points were designed based on the existing exposed rock in the soil map database from HueGIS data, compared with the possibility of exposed rock classification from Sentinel-2A and Landsat 8 under field-deployable conditions. Twelve survey points were conducted at test site 1 (A Luoi) and the other 11 points were surveyed at test site 2 (Nam Dong) (Figure 8, 9).

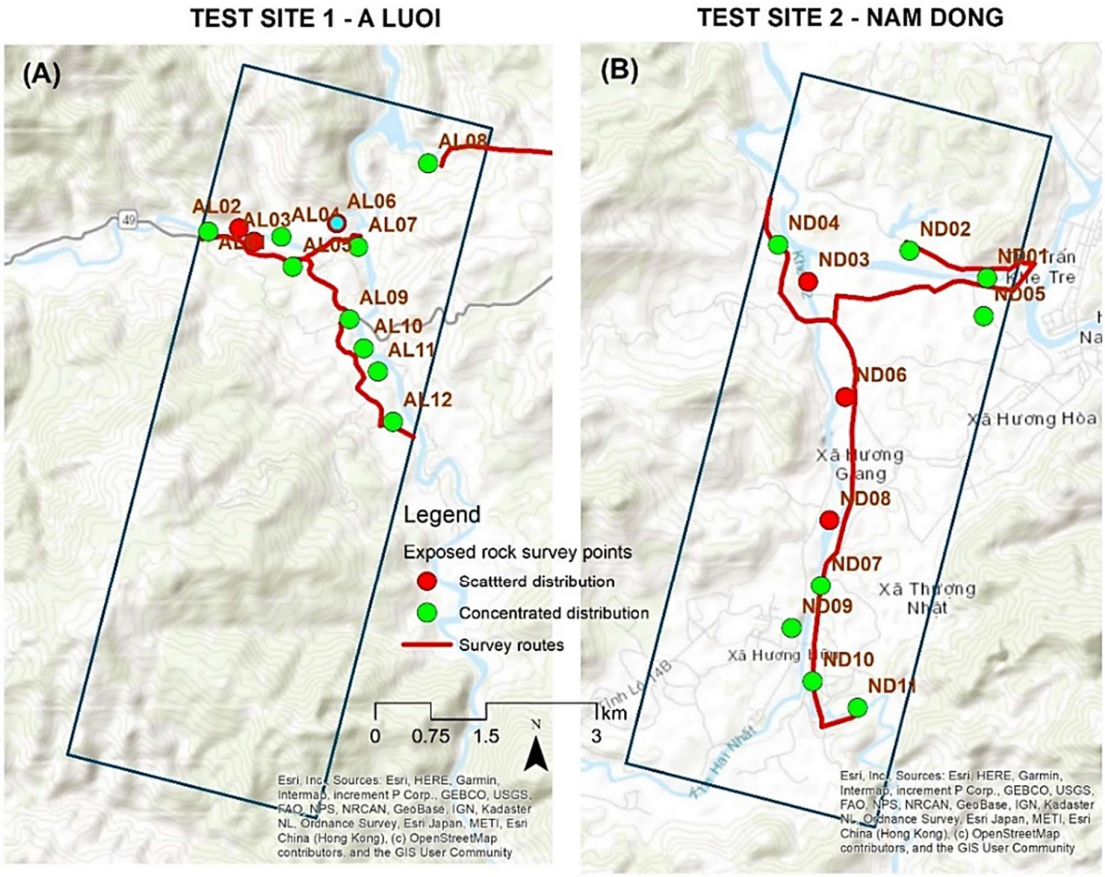

Figure 8 Map of the field survey for validating the accuracy of exposed rock extraction from Sentinel-2A and Landsat 8 in the mountainous areas: (A) test site 1- A Luoi and (B) test site 2 - Nam Dong.

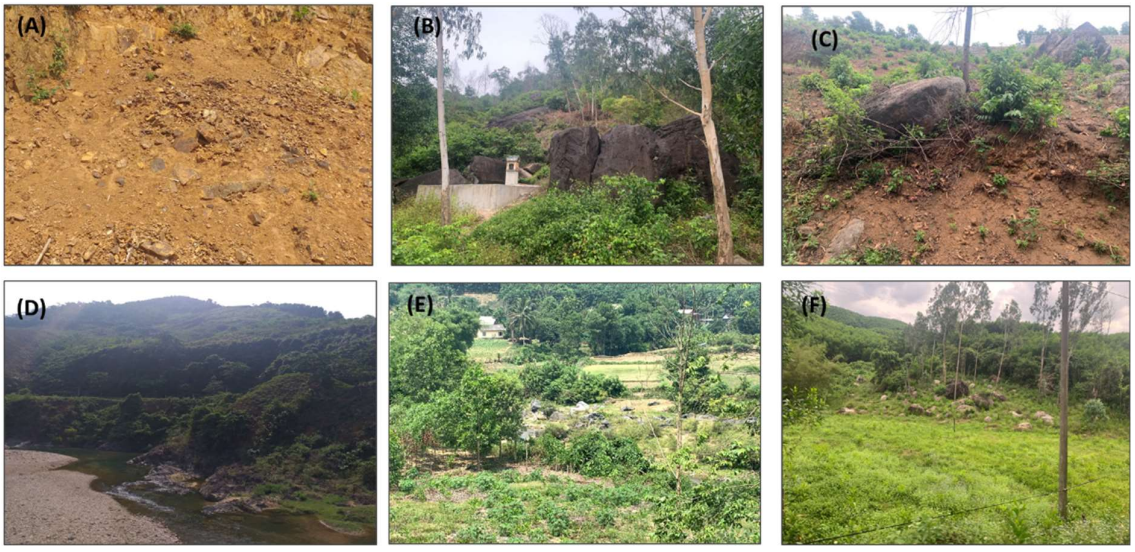

Figure 9 Landscape of rock outcrops in mountainous areas: concentrated distribution in bare land (A); in the residential area (B); on rocky slopes (C); scattering distribution along streams and rivers (D); in the cultivated area (E); and plantation forests (F).

The interpretation of the comparison between exposed rock identification results from the field survey, existing datasets, and Landsat 8 and Sentinel-2A OBOC classification are summarised in Table 5.

Table 5 Comparison of exposed rock identification results from the field survey, existing datasets, and Landsat 8 and Sentinel-2A OBOC classification.

Test site 1					Test site 2				
	Rock outcrop occurrence (√: yes, o: No)								
Survey point	In the field	Existing GISHue database	OBOC classification		Survey point	In the field	Existing GISHue database	OBOC classification	
			Landsat 8	Sentinel-2				Landsat 8	Sentinel-2
AL01	√	√	√	√	ND01	√	√	√	√
AL02	√	√	√	√	ND02	√	√	o	√
AL03	√	√	›	o	ND03	√	o	√	√
AL04	√	√	√	√	ND04	√	√	o	√
AL05	√	√	√	√	ND05	√	√	√	√
AL06	√	√	›	√	ND06	√	o	√	√
AL07	√	o	√	√	ND07	√	√	o	√
AL08	√	√	√	√	ND08	√	√	o	√
AL09	√	√	√	√	ND09	√	o	√	√
AL10	o	√	›	o	ND10	√	√	√	√
AL11	o	o	›	o	ND11	√	√	o	√
AL12	o	√	›	o					

Table 5 lists the actual test sites considering the outcrop rocks present in the study area. Only 20/23 points in the existing GISHue database contained outcrops, and there were areas at AL10-AL12 that showed no outcrops depicted in the data. The results of outcrop rock extraction for Landsat 8 data were accurate (13/23 points compared to reality) and exhibited an 83% similarity with the GISHue database. On the other hand, outcrop data extracted from Sentinel-2A data showed a 93% agreement with GISHue data and a 17/23-point overlap with reality. Furthermore, Sentinel-2A data revealed specific sites with outcrop rocks not included in the data, yet which yielded reliable field results.

In terms of the analytical findings, there were no precisely exposed rock areas in the data because the soil map was created in 2003. There were numerous alterations due to human effects that could not be added throughout time. On the one hand, the impact of separate bands, which resulted in varied ratio pictures, making the distinction between objects located in the same direction complex, could explain the discrepancies between Sentinel-2A and Landsat 8 interpretations. The test site 2 location, for example, has an open quarry and is surrounded by raw land, but the Landsat 8 image indicated that it is a developed area. Sentinel-2A delivered a more accurate interpretation than Landsat 8, as proven by field testing and the use of Google Earth Ground Truth.

On the other hand, TGSI also showed that it is essential in determining and increasing the accuracy of exposed rock fragments at all stages of the process. Other items such as vegetated objects and water impacted the rock exposure during implementation, but this was resolved/enhanced by other indications (NDVI, NDBI). The TGSI equation attempts to distinguish between surface area and bare ground. The difference is due to the different reflections of items to the Red, Blue, and Green band values, with plants and water having negative or small discounts and bare objects having greater values, allowing for the identification of exposed surface textures.

The research on extracting exposed rocks is an essential task in establishing a soil map database for agricultural development, especially in the mountainous areas of the Thua Thien Hue province. To the best of our knowledge, there have been no previous studies applying remote sensing imaging to map exposed rocks in Vietnam. Our results suggest that using Sentinel-2A images to extract mantle layers, and tiny and scattered objects such as exposed rocks in mountainous areas is better than using Landsat image using the OBOC method which integrates multiple ratio image indices (NDVI, NDBI, TGSI).

The ability to map outcrop rocks depends mainly on the surrounding landscape conditions and the characteristics of the outcrop. Therefore, the extraction method and the appropriate remote sensing image data show differences in the various studied cases. Highly heterogeneous karst regions in Du'an, Guangxi Province, southwestern China are heavily influenced by terrain relief in a particular environment formed within carbonate bedrock. The dimidiate pixel model and spectral mixture analysis approaches were selected to explore their capabilities in rocky karst desertification monitoring [25]. Meanwhile, for Antarctica, an area that is covered with snow and glaciers all year, the band ratio method was used for exposed rock extraction and mapping using Landsat 8 images. An exposed rock extraction index was built and a threshold was determined based on the spectral difference between the reflectance of NIR and SWIR2 with a high accuracy [9]. Even in weathered and vegetated coastal zones, such as in Southern China, lithological mapping has been conducted using Sentinel-2A and ASTER GDEM data based on the fractal "DN-A" (digital number-area) algorithm in conjunction with spectral indices

(NDVI, NDSI, MNSWI) and terrain analyses. The appropriate threshold could yield accurate detection results on lithology by applying the fractal concentration-area algorithm [23].

The above case studies considered territorial conditions which were different from the hilly and mountainous area studied here, affecting the selection of remote sensing data, approaches, and interpretation algorithms. While mountainous karst areas, coastal areas, or Antarctica have typical vegetation covers and exposed rocks separated from other vegetation cover types, the mountainous area considered here has a tropical climate affected by monsoons. The characteristics of the study area include scattered exposed rocks mixed with different vegetation covers, bare land, residential areas, and water bodies. Therefore, this study mainly focuses on the experimentation in image analysis with a thresholding algorithm, combined with an understanding of the geographical conditions of the research territory and expert knowledge of context to improve the accuracy in building outcrop rock maps in this specific study.

5. Conclusion

This study investigated the capability of recovering rock outcrop information from Sentinel-2A and Landsat 8 data for the mountainous areas of Vietnam to lay the foundation for future object extraction research. The use of Sentinel-2A and Landsat 8 imagery to extract rock outcrops using the OBOC method and index images was examined. The analysis found that free accessible remote sensing data sources facilitate conducting a preliminary study to analyse surface objects.

The overall accuracy of the rock outcrop objects from Landsat 8 and Sentinel-2A images was greater than 80%. The information extraction of built-up lands, bare ground, and specifically exposed rocks differed substantially from the image bands and index image values.

The findings suggest that Sentinel-2A data is more accurate than Landsat 8 data, although the extraction of information based on the rule set is highly dependent on the accuracy of the threshold or the specification of the indicators' input number. One of the essential aspects of retrieving outcrop information from remote sensing data is the TGSI. The results also revealed that the TGSI considerably contributed to the accuracy of rock outcrop classification. The TGSI is recommended for bare land identification, particularly to identify rock outcrops that appear as tiny objects that are otherwise difficult to detect with other ratio pictures in mountainous areas.

6. Acknowledgments

We are grateful to the Project entitled Study on the application of Remote Sensing and GIS to build Geodatabase of Soil and Engineering Soil/Ressources, Case study of Thua Thien Hue province Code VT-UD.09/17-20 for supporting this work. We also would like to acknowledge the constructive and valuable comments, suggestions from the anonymous Reviewers and Editors.

7. References

[1] Menegoni N, Giordan D, Perotti C, Tannant DD. Detection and geometric characterization of rock mass discontinuities using a 3D high-resolution digital outcrop model generated from RPAS imagery - Ormea rock slope, Italy. Eng Geol. 2019;252:145-163.

[2] Mohajane M, e. Land Use/Land Cover (LULC) using Landsat data series (MSS, TM, ETM+ and OLI) in Azrou Forest, in the Central Middle Atlas of Morocco. Environments. 2018;5:231-247.

[3] Tuan NQ, Huong DTV, Phong DNN, Van ND. Possibility for identifying/extracting rock outcrop using Landsat 8 OLI/TIRS - Case study of Thua Thien Hue Province. VNU J Sci: Earth Environ Sci. 2020;36(3):102-115. (In Vietnamese)

[4] Korhone L, Hadi, Packalen P, Rautiainen M. Comparison of Sentinel-2 and Landsat 8 in the estimation of boreal forest canopy cover and leaf area index. Remote Sens Environ. 2017;195:259-274.

[5] Labib SM, Harris A. The potentials of Sentinel-2 and Landsat-8 data in green infrastructure extraction, using object-based image analysis (OBIA) method. Eur J Remote Sens. 2018;51:231-240.

[6] Van der Werff H, Van der Meer F. Sentinel-2A MSI and Landsat 8 OLI provide data continuity for geological remote sensing. Remote Sens. 2016;8(11):883.

[7] Cardoso-Fernandes J, Teodoro AC, Lima A, Perrotta M, Roda-Robles E. Detecting lithium (Li) mineralizations from space: Current research and future perspectives. Appl Sci. 2020;10:1785.

[8] Gebru BM, Lee WK, Khamzina A, Wang SW, Cha S, Song C, et al. Spatiotemporal multi-index analysis of desertification in dry Afromontane forests of northern Ethiopia. Environ Dev Sustain. 2020;20:587-605.

[9] Kang J, Cheng X, Hui F, Ci T. An accurate and automated method for identifying and mapping exposed rock outcrop in Antarctica using Landsat 8 images. IEEE J Sel Top Appl Earth Obs Remote Sens. 2018;11:57-67.

[10] Xiao J, Shen Y, Tateishi R, Bayaer W. Development of topsoil grain size index for monitoring desertification in arid land using remote sensing. Int J Remote Sens. 2006;27(12):2411-2422.
[11] Yue YM, Wang KL, Liu B, Li R, Zhang B, Chen HS, et al. Development of new remote sensing methods for mapping green vegetation and exposed bedrock fractions within heterogeneous landscapes. Int J Remote Sens. 2013;34(14):5136-5153.
[12] Bachri I, Hakdaoui M, Raji M, Teodoro AC, Benbouziane A. Machine learning algorithms for automatic lithological mapping using remote sensing data: A case study from Souk Arbaa Sahel, Sidi Ifni Inlier, Western Anti-Atlas, Morocco. ISPRS Int J Geo-Inf. 2019;8:248-261.
[13] Balková M, Bajer A, Patočka Z, Mikita T. Visual exposure of rock outcrops in the context of a forest disease outbreak simulation based on a canopy height model and spectral information acquired by an unmanned aerial vehicle. ISPRS Int J Geo-Inf. 2020;9:325-332.
[14] Zha Y, Gao J, Ni S. Use of normalized difference built-up index in automatically mapping urban areas from TM imagery. Int J Remote Sens. 2003;24(3):583-594.
[15] Tuan NQ, Thu BT, Hanh HV, Thien QD, Huong DTV, Trong TD, et al. Study on the application of remote sensing and GIS to build database of soil and engineering soil resources. National Projects. Viet Nam; 2020. (In Vietnamese)
[16] People's Committee of Thua Thien Hue Province. Geography of Thua Thien Hue - Part 1. Vietnam: Social Science Publishing House; 2005. p. 68-85.
[17] Lamchin M, Lee JY, Lee WK, Lee EJ, Kim M, Chul-Hee L, et al. Assessment of land cover change and desertification using remote sensing technology in a local region of Mongolia. Adv Space Res. 2016;57:64-77.
[18] Novelli A, Aguilar MA, Nemmaoui A, Aguilar FJ, Tarantinoa E. Performance evaluation of object based greenhouse detection from Sentinel-2 MSI and Landsat 8 OLI data: A case study from Almería (Spain). Int J Appl Earth Obs Geoinf. 2016;52:403-411.
[19] Tamta K, Bhadauria HS, Bhadauria AS. Object-Oriented approach of information extraction from high-resolution satellite imagery. IOSR J Comput Eng. 2015;17(3):47-52.
[20] Bhandari AK, Kumar A, Singh GK. Feature extraction using normalized difference vegetation index (NDVI): A case study of Jabalpur City. Proc Technol. 2012;6:612-621.
[21] Rousse JW, Haas RH, Schell JA, Deering DW. Monitoring vegetation systems in the great plains with ERTS. 3rd Earth Resources Technology Satellite1 Symposium; 1973 Dec 10-14; Washington, USA. p. 309-317.
[22] Xi Y, Thinh NX, Li C. Preliminary comparative assessment of various spectral indices for built-up land derived from Landsat-8 OLI and Sentinel-2A MSI imageries. Eur J Remote Sens. 2019;52(1):240-52.
[23] Lin J, Wang R, Zhao B, Cheng S. A comprehensive scheme for lithological mapping using Sentinel-2A and ASTER GDEM in weathered and vegetated coastal zone, southern China. Open Geosci. 2019;11:982-996.
[24] Congalton RG. A review of assessing the accuracy of classifications of remotely sensed data. Remote Sens Environ. 1991;37:35-49.
[25] Qi X, Zhang C, Wang K. Comparing methods of rocky desertification monitoring at the sub-pixel scale in a highly heterogeneous karst region. Preprints. 2018;02:169-189.